Electronic Fine Tuning of the Structures of Reduced Rare-Earth Metal Halides

Martin Köckerling*,† and James D. Martin*,‡

Institut für Synthesechemie, Fachbereich 6-Festkörperchemie, Gerhard-Mercator-Universität, Lotharstrasse 1, D-47057 Duisburg, Germany, and Department of Chemistry, North Carolina State University, Raleigh, North Carolina 27695

Received August 30, 2000

Electronic band-structure calculations on Pr_3I_3Ru and Y_3I_3Ru have been performed in order to analyze the large structural differences found in these isoelectronic compounds. These constitute two structural extremes within the family of monoclinic RE_3I_3Ru phases (RE = rare-earth metal) that exhibit distortions ranging from one-dimensional double chains of trans-edge-sharing octahedra (bioctahedral chains, BOH) to one-dimensional chains of trans-edge-sharing square pyramidal units bonded base to base (bisquare pyramidal chains, BSP). The structure of La_3I_3Ru was established by single-crystal X-ray diffraction (monoclinic, $P2_1/m$, $Z = 4$, $a = 9.343(1)$ Å, $b = 4.3469(8)$ Å, $c = 12.496(3)$ Å, $\beta = 93.42(2)°$) and found to be isomorphous with the BOH Pr_3I_3Ru. It is determined that the structural variation in this RE_3I_3Z family of materials depends largely on the differences in orbital energies between the corresponding rare-earth metal and the interstitial. These bonding considerations can be generalized to account for structural variations in a variety of other rare-earth halides as well as several group 4 or 5 reduced metal halide cluster phases.

Introduction

Solid-state synthetic investigations of reduced rare-earth (RE) metal halides have revealed an exceedingly rich cluster chemistry that is based on $RE_6X_{12}Z$ metal octahedra as the basic building blocks.[1−3] Whereas most of the reduced halides of groups 4 and 5 metals contain well-isolated octahedra, condensation through trans edges into oligomeric units, chains, or networks is quite often observed for group 3 metal halides. With a few exceptions that are pure binary phases (for example, RE_2X_3, RE_2X_5 (X = Cl, Br, I),[4] and LaI[5] or LaI_2[6]) a majority of the reduced rare-earth metal halides phases contain heteroelement interstitials, Z, to stabilize the RE_6 octahedra. These include main group elements H, B−N, Si, etc., C_2 units, and also late transition metals from all three periods Mn−Cu, Ru−Pd, and Re−Au. In the domain of structures that contain one-dimensional infinite chains of condensed clusters, distinct families are found with the compositions RE_4I_4Z,[7] RE_4I_5Z,[8−11] the monoclinic members of RE_3X_3Z (X = I, Br, Cl; Z = Mn, Ru, Os, Ir, C),[9,12,14−17] Sc_5Cl_8Z (Z = C, N),[18] Sc_4Cl_6Z (Z = B, N),[19] $Sc_7Cl_{10}C_2$,[20] $Y_6I_7C_2$,[11] $Y_{10}I_{13}C_2$,[21] and $Gd_{12}I_{17}C_6$.[22] However, within the compositional boundary of the RE_3X_3Z family, compounds are found with dramatically distinct structures for apparently isoelectronic materials. For example, La_3I_3Os[23] adopts a cubic, three-dimensionally condensed structure, whereas La_3I_3Ru exhibits the monoclinic bioctahedral chain structure (BOH) and Y_3I_3Ru[12] is found to crystallize with a bisquare pyramidal chain distortion (BSP). Interestingly, Pr_3I_3Os has been found to crystallize with each of the cubic and BOH-chain morphologies.[9,23a] Similarly, the compound La_4I_5Ru[8] exhibits a structure with a single chain of condensed octahedra whereas the isoelectronic yttrium-based material forms a condensed cluster $Y_{16}I_{20}Ru_4$.[24] Clearly, subtle variations in the bonding requirements of the constituent elements are responsible for

† Gerhard-Mercator-Universität.
‡ North Carolina State University.

(1) Corbett, J. D. *J. Alloys Compd.* **1995**, *229*, 10.
(2) (a) Corbett, J. D. In *Modern Perspectives in Inorganic Crystal Chemistry*; Parthé, E., Ed.; NATO ASI Series C.; Kluwer Academic Publishers: Dordrecht, The Netherlands, 1992; p 27. (b) Corbett, J. D. *J. Chem. Soc., Dalton Trans.* **1996**, 575.
(3) Simon, A.; Mattausch, Hj.; Miller, G. J.; Bauhofer, W.; Kremer, R. K. In *Handbook on the Physics and Chemistry of Rare Earths*; Gschneider, K. A., Jr., Eyring, L., Eds.; Elsevier Science: Amsterdam, 1991; Vol. 15, p 191.
(4) Meyer, G. *Chem. Rev.* **1988**, *88*, 93 and references therein.
(5) Martin, J. D.; Corbett, J. D. *Angew. Chem.* **1995**, *107*, 234.
(6) (a) Corbett, J. D.; Sallach, R. A.; Lokken, D. A. *Adv. Chem. Ser.* **1967**, *71*, 56. (b) Warkentin, E.; Bärninghausen, H. *Z. Anorg. Allg. Chem.* **1979**, *459*, 187.
(7) Dorhout, P. K.; Corbett, J. D. *J. Am. Chem. Soc.* **1992**, *114*, 1697.
(8) Payne, M. W.; Dorhout, P. K.; Corbett, J. D. *Inorg. Chem.* **1991**, *30*, 1467.
(9) Park, Y.; Martin, J. D.; Corbett, J. D. *J. Solid State Chem.* **1997**, *129*, 277.
(10) Nagaki, D.; Simon, A.; Borrmann, H. *J. Less-Common Met.* **1989**, *156*, 193.
(11) Kauzlarich, S. M.; Hughbanks, T.; Corbett, J. D.; Klavins, P.; Shelton, R. N. *Inorg. Chem.* **1988**, *27*, 1791.
(12) Payne, M. W.; Dorhout, P. K.; Kim, S.-J.; Hughbanks, T. R.; Corbett, J. D. *Inorg. Chem.* **1992**, *31*, 1389.
(13) West, R. C., Ed. *CRC Handbook of Chemistry and Physics*, 65th ed.; CRC Press: Boca Raton, FL, 1985; pp E63, E64.
(14) Ebihara, M.; Martin, J. D.; Corbett, J. D. *Inorg. Chem.* **1994**, *33*, 2079.
(15) Mattausch, Hj.; Kremer, R. K.; Simon, A.; Bauhofer, W. *Z. Anorg. Allg. Chem.* **1993**, *619*, 741.
(16) Mattausch, Hj.; Schwarz, C.; Simon, A. *Z. Kistallogr.* **1987**, *178*, 156.
(17) Llusar, R.; Corbett, J. D. *Inorg. Chem.* **1994**, *33*, 849.
(18) Hwu, S.-J.; Dudis, D. S.; Corbett, J. D. *Inorg. Chem.* **1987**, *26*, 469.
(19) Hwu, S.-J.; Corbett, J. D. *J. Solid State Chem.* **1986**, *64*, 331.
(20) Hwu, S.-J.; Corbett, J. D.; Poeppelmeier, K. R. *J. Solid State Chem.* **1985**, *57*, 43.
(21) Kauzlarich, S. M.; Payne, M. W.; Corbett, J. D. *Inorg. Chem.* **1990**, *29*, 3777.
(22) Simon, A.; Warkentin, E. *Z. Anorg. Allg. Chem.* **1983**, *497*, 79.
(23) (a) Dorhout, P. K.; Payne, M. W.; Corbett J. D. *Inorg. Chem.* **1991**, *30*, 4960. (b) For further members of this family of compounds see the following. Nagaki, D.; Simon, A.; Borrmann, H. *J. Less-Common Met.* **1989**, *156*, 193. Warkentin, E.; Simon, A. *Rev. Chim. Miner.* **1983**, *20*, 488.
(24) Payne, M. W.; Ebihara, M.; Corbett J. D. *Angew. Chem.* **1991**, *103*, 842.

10.1021/ic000986d CCC: $20.00 © 2001 American Chemical Society
Published on Web 12/16/2000

Table 1. Selected Data Collection and Refinement Parameters for La_3I_3Ru

space group; Z	$P2_1/m$ (No. 11); 2
a (Å)	9.343(1)
b (Å)	4.3469(8)
c (Å)	12.496(3)
β (deg)	93.42(2)
V (Å^3)	506.6(2)
no. of obsd reflns ($I_o > 2\sigma(I_o)$); variables	731; 44
μ (Mo Kα; cm^{-1})	229.1
transm factor range	0.9472−1.0000
R^a	0.0229
$R_w{}^b$	0.0265

[a] $R_1 = \sum||F_o| - |F_c||/\sum|F_o|$. [b] $R_w = \{[\sum w(|F_o| - |F_c|)^2]/\sum w(F_o)^2\}^{1/2}$. $w = 1/(\sigma^2(F_o) + (0.01\ F_o)^2)$.

remarkable structural distortions in these systems. In this present work we demonstrate that these distortions within isoelectronic structural families can reasonably be traced to the relative orbital energies (electronegativities) of the respective rare-earth and interstitial elements.

Experimental Section

General Techniques. Because of the air and moisture sensitivity of the reactants and products, all manipulations were carried out under vacuum or inert gas. Preparative techniques for the high-temperature synthesis of new rare-earth metal halides using welded niobium tubing are described in ref 25. X-ray powder patterns were obtained using an Enraf-Nonius Guinier camera with monochromated Cu Kα radiation ($\lambda = 1.540\ 562$ Å) and were used for phase identification by comparison of their patterns with those calculated on the basis of single-crystal data for prototype structures. Phase yields were estimated according to the relative intensity distribution on the Guinier films as well as by careful examination of the bulk product. Precise lattice parameters were obtained by least-squares refinements of the positions of indexed reflections using Si as an internal standard.

Synthesis. La_3I_3Ru was first observed in powder patterns of several exploratory reactions loaded in the quaternary A−La−I−Ru system (A = alkaline metal) in the search for new lanthanum iodide cluster structures. However, La_3I_3Ru is prepared in high yield from the combination of La metal (Ames Lab, >99.9% metal purity), LaI_3 (sublimed), Ru metal (Johnson-Matthey, >99.9% metal purity) in a 2:1:1 mole ratio. Reactions were typically run on a 300 mg scale. The reactants were welded into Nb tubes, which in turn were encapsulated in evacuated silica jackets. The reaction vessels were heated to 900 °C for 7 weeks. This reaction yielded X-ray quality single crystals in near quantitative yield. The yield of the RE_3I_3Z phases is generally enhanced by La- and/or Z-rich loadings (~5% excess), though more metal-rich loadings result in the formation of La_2IRu or La_2IRu_2.[9]

X-ray Structure Determination. A black single crystal of La_3I_3Ru (size: 0.04 mm × 0.04 mm × 0.25 mm) was fixed with grease inside a 0.3 mm Lindemann capillary and flame-sealed. On a Rigaku AFC6R diffractometer 15 reflections were centered in the range 12−18° in 2θ. These were indexed to a monoclinic cell with the lattice constants $a =$ 9.343(1) Å, $b = 4.3469(8)$ Å, $c = 12.496(3)$ Å, $V = 506.6(2)$ Å^3, and $Z = 4$. One hemisphere of data, $2\theta \le 50°$, was collected at ambient temperature. An empirical absorption correction was applied to the data using the average of three ψ-scan reflections. The structure was solved using direct methods (SHELX-86).[26] The anisotropic refinement converged at R; $R_w = 2.27$, 2.62%. The largest residual in the final difference Fourier map was a peak of 1.12 e/Å^3, 1.49 Å from I1. A summary of crystallographic data is given in Table 1. Full details of the structural determination are available in the Supporting Information or from the authors.

Table 2. Atomic Orbital Parameters Employed in the EH Calculations

atom	orbital	H_{ii} [eV]	$\zeta1^a$	c1[b]	$\zeta2^a$	c2[b]
Pr[29]	6s	−4.890	1.377	1.0		
	6p	−3.320	1.377	1.0		
	5d	−6.350	2.779	0.5766	1.404	0.4641
Y[30]	5s	−7.020	1.740	1.0		
	5p	−4.400	1.700	1.0		
	4d	−6.800	1.560	0.8215	3.554	0.3004
Ru[31,32]	5s	−7.293	2.08	1.0		
	5p	−4.022	2.04	1.0		
	4d	−11.533	5.58	0.5343	2.300	0.6368
I[31,32]	5s	−21.069	2.68	1.0		
	5p	−11.561	2.32	1.0		

[a] Coefficients used in the single-ζ or double-ζ expansions. [b] Slater-type orbital exponents.

Table 3. Positional and Isotropic-Equivalent Thermal Parameters for La_3I_3Ru

atom	x	y	z	$U_{eq}{}^a$
La1	0.09766(8)	0.25	0.89152(6)	0.0174(2)
La2	0.12057(8)	0.25	0.33723(6)	0.0194(3)
La3	0.31863(8)	0.75	0.12271(6)	0.0172(3)
I1	0.39138(9)	0.75	0.86265(7)	0.0214(3)
I2	0.3774(1)	0.75	0.38335(7)	0.0249(3)
I3	0.1377(1)	0.25	0.61825(7)	0.0224(3)
Ru1	0.1144(1)	0.25	0.12623(9)	0.0156(3)

[a] $U_{eq} = {}^1/_3\sum_i\sum_j U_{ij}a_i^*a_j^* \times \vec{a}_i\vec{a}_j$.

Electronic Structure Calculations. Calculations by the extended Hückel tight binding method[27] were done with the aid of the EHMACC program, adapted to an IBM-compatible PC.[33] Calculations were carried out on isolated one-dimensional chains in which all interchain bridging iodides were replaced with terminal iodides to yield the repeat unit $[RE_6I_{10}Z_2]^{4-}$ for both the BOH-Pr_3I_3Ru and the BSP-Y_3I_3Ru structure using crystallographic coordinates.[12] The atomic orbital parameters employed in the calculations are summarized in Table 2. To model the effect of different ionization energies of the different rare-earth metals, calculations were also performed using the Y parameters for the BOH structure (Y orbitals and energies and Y energies with Pr orbitals) and the Pr parameters for the BSP-metal arrangement (Pr orbitals and energies and Pr energies with Y orbitals). The one-dimensional calculations were carried out with 100K points. Crystal orbital overlap population (COOP) plots for the different types of interactions within each compound are put onto one common scale to make them comparable.

Results and Discussion

Structure of La_3I_3Ru. The structure of La_3I_3Ru was found to be isostructural with Pr_3I_3Ru. The atomic coordinates and isotropic-equivalent thermal parameters for La_3I_3Ru are given in Table 3, and the important distances appear in Table 4. This BOH structure contains infinite double chains of trans-edge-condensed octahedra, which run along the crystallographic b

(25) Corbett J. D. In *Solid State Chemistry: Techniques*; Cheetham, A. K., Day, P., Eds.; Clarendon Press: Oxford, 1987; Chapter 1, p 1 ff.
(26) Sheldrick, G. M. *SHELX-86*; Institut für Anorganische Chemie, Universität Göttingen: Göttingen, Germany, 1986.
(27) (a) Whangbo, M.-H.; Hoffmann, R. *J. Am. Chem. Soc.* **1978**, *100*, 6093. (b) Ammeter, J. H.; Bürgi, H.-B.; Thibeault, J. C.; Hoffmann, R. *J. Am. Chem. Soc.* **1978**, *100*, 3686.
(28) Pearson, W. B. *The Crystal Chemistry and Physics of Metals and Alloys*; Wiley-Interscience: New York, 1972; p 151.
(29) Pyykkö, P.; Lohr, L. L., Jr. *Inorg. Chem.* **1981**, *20*, 1950.
(30) Hughbanks, T.; Corbett, J. D. *Inorg. Chem.* **1989**, *28*, 631.
(31) Vela, A.; Gázquez, J. L. *J. Phys. Chem.* **1988**, *92*, 5688.
(32) Clementi, E.; Roetti, C. *At. Data Nucl. Data Tables* **1974**, *14*, 177.
(33) Whangbo, M.-H.; Hoffmann, R.; Hughbanks, T.; Kertesz, M.; Wijeyesekera, S.; Wilker, C.; Zheng, C.; Evain M. *EHMACC: A Program for Extended Hückel Molecular and Crystal Calculations*; Department of Chemistry, Cornell University, Ithaca, NY, and Department of Chemistry, North Carolina State University, Raleigh, NC, 1987 (PC adaption by Köckerling, M. Solid State Chemistry Department, University of Duisburg, 1996).

Table 4. Important Interatomic Distances (Å) for La_3I_3Ru[a]

La−La			La−I		
La1−La1		3.999(2)	La1−I1	×2	3.536(1)
La1−La2	×2	4.044(1)	La1−I3		3.457(1)
La1−La3	×2	3.883(1)	La2−I2	×2	3.263(1)
	×2	4.077(1)	La2−I3		3.506(1)
La2−La3	×2	3.991(1)		×2	3.319(1)
$\bar{d}$		3.999	La3−I1		3.359(1)
				×2	3.470(1)
La−Ru			La3−I2		3.270(1)
La1−Ru1	×2	2.941(1)	$\bar{d}$		3.397
		2.928(1)			
La2−Ru1		2.634(1)			
La3−Ru1	×2	2.894(1)			
$\bar{d}$		2.872			

[a] All atoms have two neighbors of the same kind at $\pm b$, 4.347 Å.

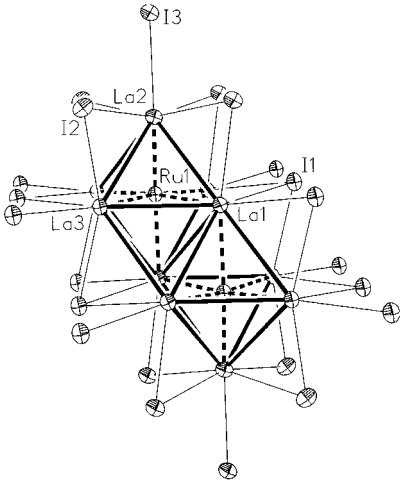

Figure 1. Section of the condensed cluster chain in La_3I_3Ru viewed slightly off [010]. La−La and La−Ru (hatched) bonding is emphasized. Atoms are presented as thermal ellipsoids with 70% probability.

axis. These chains can also be imagined to result from the side-by-side condensation of two single chains of octahedra seen in La_4I_5Ru,[8−11] which have been displaced by $b/2$ relative to each other. Iodine atoms form a sheath around the metal double chains bridging all exposed cluster edges and interbridging between chains. Figure 1 shows an off-axis view of a section of such a double chain in La_3I_3Ru.

Structural Variations within the Monoclinic Series of RE_3I_3Z Compounds. Comparison of the various members of the monoclinic RE_3I_3Z family of cluster compounds shows a more or less continuous range of structural distortions. Views of two extremes of this structural distortion are shown in Figure 2. The cluster chains of Pr_3I_3Ru or La_3I_3Ru (Figure 2A) are best described as one-dimensional chains of trans-edge-sharing Z-centered (here, Ru) metal octahedra surrounded by iodine atoms (BOH-bioctahedral). The discrete rare-earth octahedral units are no longer obvious in Y_3I_3Ru or Gd_3I_3Mn (Figure 2B). Rather, a description as the condensation of two one-dimensional chains of trans-edge-sharing square pyramidal RE_5Z units bonded base to base seems more suitable (BSP-bisquare pyramidal). The distorted chain structure can also be regarded as originating from ideal double octahedra in which one RE_5Z unit was systematically displaced along the crystallographic *a* direction relative to the second unit.[12] Virtually no displacement is observed along *b*, the chain axis, as seen by the [100] view of the Pr_3I_3Ru and Y_3I_3Ru chains in parts A and B of Figure 3. On distortion toward the square pyramidal arrangement, the apex−Z−apex angle (RE2−Z−RE1) in each octahedral chain decreases as well as the interstitial−interstitial distance, whereas

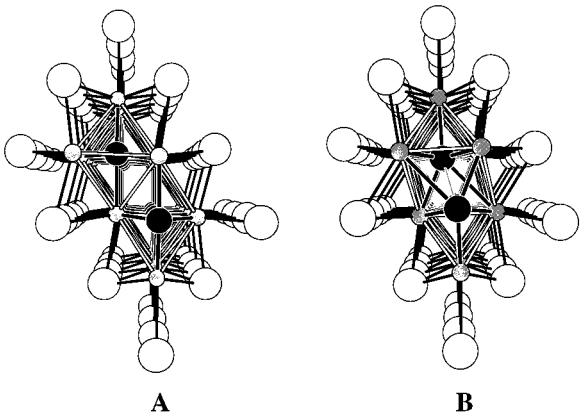

Figure 2. Approximate [010] view of two members of the monoclinic series of RE_3I_3Z compound, representing the two extremes of the structural distortion: Pr_3I_3Ru (A) defining the almost ideal BOH bioctahedral metal arrangement and Y_3I_3Ru (B) with the face-to-face-bonded BSP bisquare pyramidal metal arrangement.

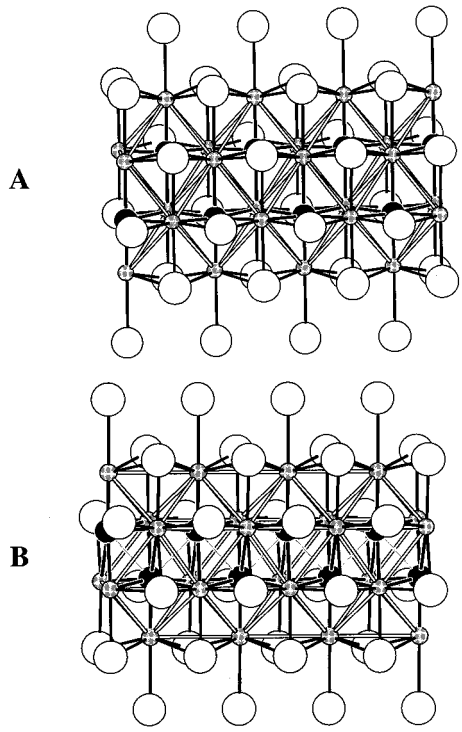

Figure 3. Side view along [100] of the clusters with BOH arrangement in Pr_3I_3Ru (A) and with BSP arrangement in Y_3I_3Ru (B).

the diagonal distance RE1−RE1 increases. The degree of distortion can be quantified by the difference between the *x* coordinates of the RE3 and RE1 atom, relative to the *a*-axis length (and multiplied by 100), described as d1 in Table 5. Taking the *a*/*b* ratio of the lattice parameters as an indicator of the distortion of compounds for which only powder-X-ray data exist, Gd_3I_3Ru is included between Pr_3I_3Ru and Y_3I_3Ru in the series of isoelectronic Ru compounds with increasing distortion toward the bipyramidal metal arrangement, and Er_3I_3Ru follows Y_3I_3Ru.[12]

To understand the driving force for this distortion, we must turn our attention to the rare-earth elements because the homologous interstitial in the Ru phases makes these materials formally isoelectronic. On comparison of the isoelectronic Pr_3I_3Ru with Y_3I_3Ru, it is striking that the average RE−RE distance decreases by ∼0.3 Å with a difference in the metallic radii of only 0.06 Å. At the same time the Ru−Ru distance

Table 5. Structural Parameters of RE_3I_3Z Compounds as Relevant for the Observed Distortions[a]

compd	av RE−RE [Å] [no./$RE_6I_6Z_2$]	av RE−Z [Å]	Z−Z [Å]	RE2−Z−RE1 [deg]
Pr_3I_3Ru	3.917 [9]	2.818	4.180	179.4
La_3I_3Ru	3.999 [9]	2.872	4.295	178.2
Gd_3I_3Ru				
Y_3I_3Ru	3.628 [8]	2.777	3.163	155.8
Er_3I_3Ru				
Pr_3I_3Os	3.922 [9]	2.825	4.144	179.7
Gd_3I_3C	3.535 [9]	2.548	3.956	169.3
Gd_3I_3Mn	3.764 [8]	2.997	2.665	145.6
Y_3I_3Ir	3.625 [8]	2.790	3.143	153.7

compd	d1[c]	r_{RE} [d] [Å]	r_Z [d] [Å]	*a*/*b*	ref
Pr_3I_3Ru	2.35	3.30	2.50	2.147	12
La_3I_3Ru	2.36	3.38	2.50	2.149	this study
Gd_3I_3Ru		3.22	2.50	2.093	12
Y_3I_3Ru	1.43	3.24	2.50	2.079	12
Er_3I_3Ru		3.14	2.50	2.074	12
Pr_3I_3Os	2.35	3.30	2.52	2.125	13
Gd_3I_3C	2.48	3.22	1.54	2.205	15
Gd_3I_3Mn	1.12	3.22	2.34	2.163	14
Y_3I_3Ir	1.26	3.24	2.54	2.051	12

[a] Gd_3I_3Ru and Er_3I_3Ru have been characterized by X-ray powder diffraction only. Thus, parameters that require atomic coordinate data are missing. [b] Without the much longer chain-repeat length. [c] Distortion parameter: $d1 = [(x(RE3) - x(RE1))/a] \times 100$. [d] Metallic radii according to Pearson.[28]

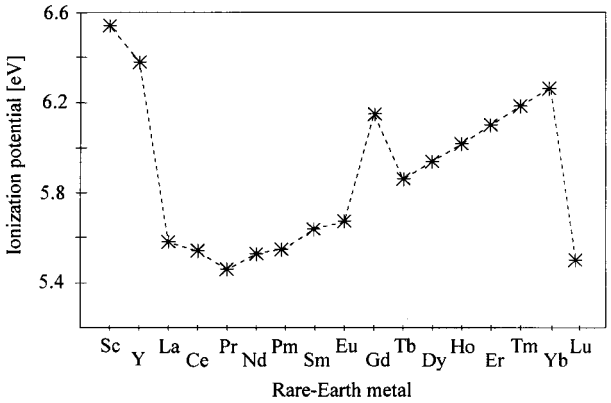

Figure 4. Variation of the first ionization energy within the group 3 lanthanide series of elements.

decreases from 4.180 to 3.163 Å. Thus, the size of the rare-earth elements does not provide a sufficient explanation for the observed distortions. Nevertheless, while formally isoelectronic, there is a significant variation in the electronic nature of the respective rare-earth elements. A plot of the first ionization energies for the rare-earth elements is given in Figure 4.[13] It thus becomes apparent that the phases that exhibit the BSP distortion (Y, Gd, and Er) have a first ionization energy of >6.0 eV whereas the nondistorted BOH structures are observed for La and Pr with first ionization energies of <5.5 eV.

Electronic Structure Analysis. To confirm and further understand the apparent structural dependence on the first ionization energy (or electronegativity) of the rare-earth element, we performed a series of band calculations to evaluate the metal−metal bonding as a function of orbital energy. Extended Hückel calculations were performed on both the BOH-Pr_3I_3Ru (for the $[^1_\infty Pr_6I_{10}Ru_2]^{4-}$ chain) and the BSP-Y_3I_3Ru ($[^1_\infty Y_6I_{10}Ru_2]^{4-}$ chain). Similar conclusions are obtained if the La structure and parameters are utilized. However, the electronic structure analysis was performed utilizing the Pr parameters and structure in order for this work to be understood in the context of previous electronic structure calculations, which have primarily focused on Pr.[12] To model the influence of the orbital energy of the rare-earth elements on the structural distortion, calculations were performed on both structure types using the orbital parameters of Y and Pr (Table 2), as well as the hypothetical parameters with the orbital exponents of Y and the H_{ii} of Pr, and orbital exponents of Pr with the H_{ii} of Y. The results of these calculations are summarized in Table 6 and Figures 5−8.

Table 6. Results from the Extended Hückel Calculations on Pr_3I_3Ru and Y_3I_3Ru

BOH-Pr_3I_3Ru Structure

	atom charges		
atom	Pr parameters	Pr orbitals Y energies	Y parameters
RE	**+1.06**	+0.76	+1.04
Ru	**−2.87**	−2.49	−2.55
I	**−0.46**	−0.35	−0.52

	overlap populations[b]		
bonds[a]	Pr parameters	Pr orbitals Y energies	Y parameters
RE-RE	**1.06**	1.66	1.18
RE-Ru	**3.53**	3.52	4.05
Ru−Ru	**0.00**	−0.01	0.00
RE−I	**7.51**	8.59	5.76

BSP-Y_3I_3Ru Structure

	atom charges		
atom	Pr parameters	Y orbitals Pr energies	Y parameters
RE	+1.04	+1.25	**+0.93**
Ru	−2.84	−2.83	**−2.38**
I	−0.46	−0.59	**−0.48**

	overlap populations[b]		
bonds[a]	Pr parameters	Y orbitals Pr energies	Y parameters
RE-RE	1.03	1.00	**1.56**
RE-Ru	3.66	3.80	**3.99**
Ru−Ru	0.09	0.12	**0.07**
RE−I	7.56	5.30	**6.26**

[a] Including all interactions up to 4.5 Å. [b] Total overlap population per $[RE_6I_{10}Ru_2]$ unit.

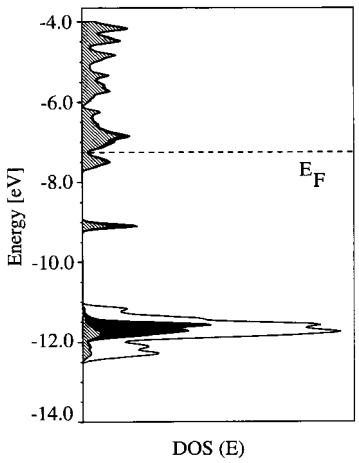

Figure 5. Total density of states (DOS) diagram for BOH-Pr_3I_3Ru with the projected DOS of Pr (hatched) and Ru (solid black).

The total density of states (DOS) for the BOH-Pr_3I_3Ru (Figure 5) shows that the Fermi level at $E_F = -7.26$ eV cuts through a local minimum, consistent with that reported in ref 12. The bands in the energy region around the Fermi level are dominated by Pr-centered orbitals, whereas Ru contributes more to the regions around −9 eV and between −11 and −12.5 eV. This

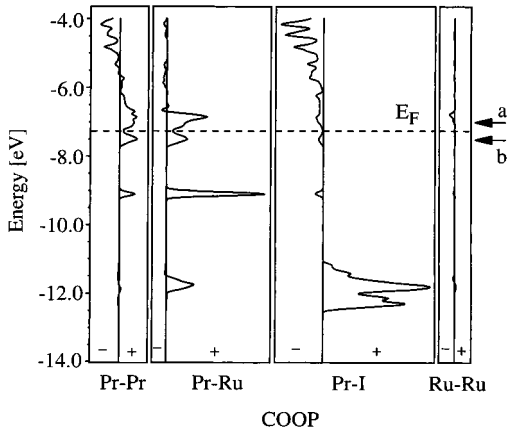

Figure 6. Averaged crystal orbital overlap population (COOP) curves for Pr−Pr, Pr−Ru, Ru−Ru, and Pr−I contacts up to 4.5 Å. Levels to the right of the vertical axes are bonding (+) while to the left are antibonding (−). The Fermi level E_F is shown as a dashed line. The arrows mark the Fermi levels for compounds with a one-electron-richer interstitial (a) or one-electron-poorer interstitial (b).

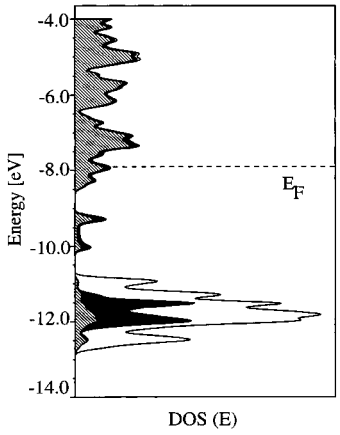

Figure 7. Total density of states (DOS) diagram for BSP-Y_3I_3Ru with the projected DOS of Y (hatched) and Ru (solid black).

picture, with essentially filled Ru orbitals, is consistent with the Ru being more electronegative than the Pr and hence the calculated charge of −2.87. The projected DOS diagram also shows some mixing of Pr levels into the I-based levels, indicating a small amount of Pr−I covalence. Analysis of the crystal orbital overlap population curves (COOP), which are given for all four types of interactions (Pr−Pr, Pr−Ru, Ru−Ru, and Pr−I) up to distances of 4.5 Å (Figure 6) provides a similar understanding of the bonding. Moderate Pr−Pr and the Pr−Ru bonding interactions are observed up to and even above the Fermi level, but no significant interstitial−interstitial bonding is observed. For comparison, arrows mark the calculated Fermi levels for isostructural systems with a one-electron-richer interstitial (level a of Figure 6), e.g. Ir, and also a one-electron-poorer interstitial (level b of Figure 6), like Mn. For the electron-rich case, interstitial−interstitial interactions would start to become sharply more antibonding above E_F, whereas the RE−RE bonding and RE−Z bonding would become even stronger.

Several features of the bonding picture are distinctly different for the BOH-Pr and BSP-Y materials. Most significantly, as seen in the plot of the DOS for BSP-Y_3I_3Ru with Y parameters (Figure 7), there is a significantly increased contribution by the rare-earth elements to the lower lying bands. In the immediate vicinity of the Fermi level (E_F = −7.91 eV) the character of the bands is still dominated by the rare-earth elements. However, the smaller difference between the orbital energy of the Y and

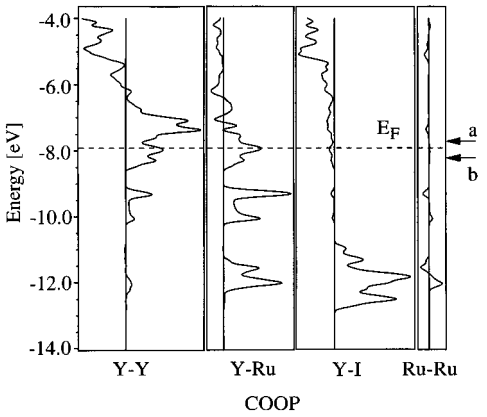

Figure 8. Averaged crystal orbital overlap population (COOP) curves for Y−Y, Y−Ru, Ru−Ru, and Y−I contacts up to 4.5 Å. Levels to the right of the vertical axes are bonding (+) while to the left are antibonding (−). The Fermi level E_F is shown as a dashed line. The arrows mark the Fermi levels for compounds with a one-electron-richer interstitial (a) or one-electron poorer interstitial (b).

Chart 1

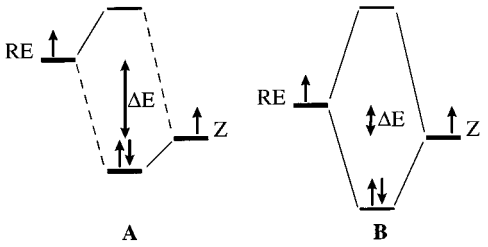

Ru results in a significant admixture of interstitial character into these bands, resulting in lower calculated charges for both elements. The increased dispersion of the metal-based bands, as well as increased relative overlap seen in the respective COOP curves (Figure 8), suggests that there is significantly increased metal−metal bonding (RE−RE and RE−Z) in the Y phase. Interestingly, the increased band dispersion in the Y phase results in the Fermi level cutting at a maximum in the DOS, suggesting that this phase may exhibit properties of a poor metal as opposed to the semiconducting behavior anticipated for the Pr phase. The lower energy of the rare-earth elements also increases the covalence of the Y−I interaction, most dramatically seen by comparison of the overlap populations for both structure types upon changing only the H_{ii} value of the RE while leaving the orbital exponents unchanged to control for the differences in atomic size (Table 6).

The driving force for the structural distortion toward the BSP structure type is readily summarized by the orbital representation in Chart 1. A large ΔE between the orbital energies of the rare-earth and interstitial elements results in significant charge transfer to the more electronegative interstitial and in a greater charge localization and thus a more ionic type of bonding. By contrast, the smaller ΔE between the rare earth and interstitial results in a significantly increased covalence of the RE−Z bonding. This is experimentally observed in the 8% contraction of the cluster unit, as seen in the RE−RE distance, on going from Pr_3I_3Ru to Y_3I_3Ru compared with the 2% decrease in their respective metallic radii (and 10% vs 2% for La vs Y). The RE−Z distances are effectively equivalent when scaled to the respective metallic radii; however, in the BSP arrangement there are seven RE−Z bonds as opposed to the six bonds in the BOH structure type. The calculated overlap populations (Pr_3I_3Ru, Pr−Pr = 1.06, Pr−Ru = 3.53, vs Y_3I_3Ru, Y−Y = 1.56 Y−Ru =

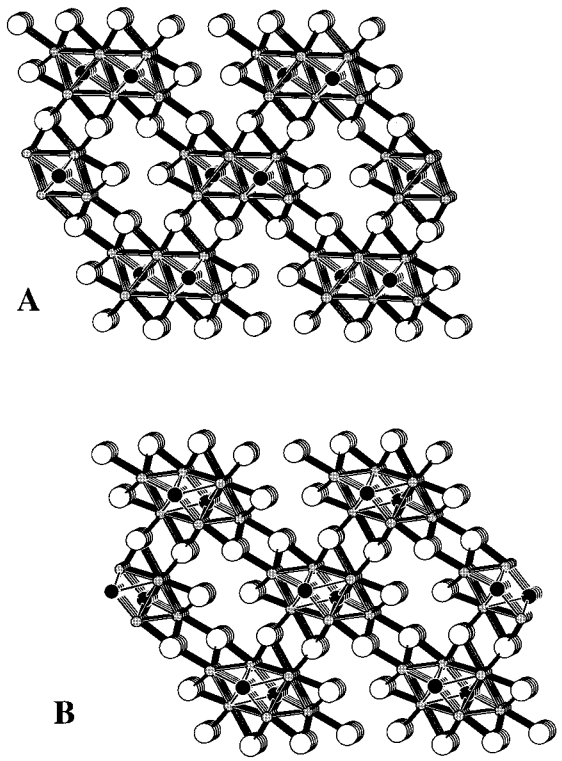

Figure 9. View of the BOH (A) and BSP (B) crystal structures emphasizing the pseudo-closest-packing of spheres in the former Pr_3I_3Ru compared with the noted distortion induced by metal−metal bonding in Y_3I_3Ru.

3.99) also confirm the increased metal−metal bonding in the yttrium phase.

While the BSP-type distortion clearly results from a maximization of the RE−RE and RE−Z bonding, why does the more idealized BOH-type structure form when only moderate metal−metal bonding is available? As indicated by Chart 1, a large ΔE between the rare-earth and interstitial elements results in significant charge transfer to the more electronegative interstitial. In our model calculations, the charge on the Ru is 20% greater for Pr_3I_3Ru than for Y_3I_3Ru. Extended Hückel calculations are known to overestimate charges, a problem that is exacerbated by the uncertainty of the parametrization; however, this trend is consistent with a comparison of the elements' respective first ionization energies or Pearsons absolute electronegativities.[35] Furthermore, the assignment of negative charge to the interstitial atoms has been shown experimentally for some zirconium clusters.[36,37] The longer Z−Z contacts in the BOH structure will result in less Coulomb repulsion with the anionic charge placed on the interstitial. Interesting too is the observation that a saltlike crystal packing, in which iodide anions and "anionic−interstitial" are nearly cubic-closest-packed and the rare-earth cations occupy $^1/_4$ of the octahedral holes (as shown in Figure 9A), is present in the BOH structure type, consistent with a more ionic bonding picture. By contrast, the increased metal−metal bonding due to the small ΔE in the yttrium/ruthenium phase destroys the saltlike packing (Figure 9B) and exhibits a notable puckering to the closest-packed-type structure.

These bonding conclusions can further be applied to understand all of the RE_3I_3Z phases reported in Table 5. For all transition metal centered phases, the more electropositive rare-earth elements (La and Pr) result in the formation of a BOH geometry whereas the more electronegative Y, Gd, and Er exhibit the distorted BSP geometry. Interestingly, in the carbon-centered Gd_3I_3C phase, however, the ΔE between Gd and C is large, and thus, the BOH geometry is observed. The added electron in the Y_3I_3Ir phase increases the electron density primarily in the RE−RE bonding states, thus also favoring the BSP geometry. The electron-deficient Gd_3I_3Mn phase exhibits the greatest distortion toward an idealized BSP geometry, giving very short Mn−Mn contacts of 2.61 Å. We observe no evidence for significant Mn−Mn bonding in this phase but rather attribute the distortion to the smaller size of the Mn interstitial (metallic radii Mn = 2.34 Å vs Ru = 2.50 Å). The smaller size of the interstitial allows strengthening of the RE−RE and RE−Z bonding without increasing the Z−Z repulsion, even though the ΔE is slightly greater for Gd/Mn than for Y/Ru.

Generalization and Outlook. The importance of the difference in orbital energies between the rare-earth elements and the interstitials for determining the observed structures of specific cluster compounds must clearly extend far beyond the RE_3I_3Z phases. As an example, we briefly consider the composition of RE_4I_5Z for which two basic structure types are observed. One is composed of single chains of edge-sharing octahedra, whereas the second structure type contains condensed $RE_{16}I_{20}Z_4$ clusters. The one-dimensional-chain structure, which is less condensed because of lesser metal−metal bonding, is found for the large ΔE phases of Pr_4I_5Z (Z = Co, Ru, Os),[8] La_4I_5Ru,[8] Gd_4I_5Si,[10] and Y_4I_5C.[11] By contrast, the condensed $RE_{16}X_{20}Z_4$ oligomers have only been found for RE = Sc, Y, and Gd; Z = Mn, Fe, Ru, and Ir; and X = I and Br,[2b,24,38−40] in which a smaller ΔE between RE and Z is observed. Furthermore, even within the mono-octahedral RE_4X_5Z-chain phases a tetragonal compression is observed, and in the $RE_{16}X_{20}Z_4$ condensed clusters a "breathing-type" distortion is observed[39] that seems to be correlated to the difference in orbital energies. We further anticipate that the ΔE between the rare earth and halide (bromide vs iodide) also plays a role in determining the chain vs oligiomer formation. These distortions will be the subject of a future detailed investigation.

An extension of this analysis may also account for the observation that ternary and quaternary interstitial-stabilized phases of groups 4 and 5 metals normally exhibit only isolated "M_6Z" cluster phases as opposed to condensed chains and clusters. The groups 4 and 5 elements are the most electronegative (highest first ionization potentials) of the cluster-forming elements and thus yield the smallest ΔE between the cluster-forming and interstitial elements. As a consequence, strong M−Z bonding is expected at the expense of significant M−M bonding, which is required for the formation of condensed phases.

The true test of any theoretical description of bonding is in its predictive ability as opposed to simply being a descriptive analysis. In this regard it is striking that a majority of the condensed (metal-rich) ternary cluster phases are found for RE = Sc, Y, and Gd,[3] which are also the rare-earth elements with relatively high first ionization energies. Thus, we suggest that the lesser explored, later rare-earth elements (Tb, Dy, Ho, Er, Tm, and Yb) are likely to form similar condensed cluster phases because their relatively high first ionization energies (see Figure 4) should yield a relatively small ΔE with transition metals as

(34) Bond, M. R.; Hughbanks, T. *Inorg. Chem.* **1992**, *31*, 5015.
(35) Pearson, R. G. *Inorg. Chem.* **1988**, *27*, 734.
(36) Ziebarth, R. P.; Corbett, J. D. *J. Am. Chem. Soc.* **1989**, *111*, 3272.
(37) Harris, J. D.; Hughbanks, T. *J. Am. Chem. Soc.* **1997**, *119*, 9449.
(38) Ebihara, M.; Martin, J. D.; Corbett, J. D. *Inorg. Chem.* **1994**, *33*, 2079.
(39) Steinwand, S. J.; Corbett, J. D.; Martin, J. D. *Inorg. Chem.* **1997**, *36*, 6413.
(40) Steinwand, S. J.; Corbett, J. D. *Inorg. Chem.* **1996**, *35*, 7056.

interstitials. By contrast, Ce, Nd, Pm, Sm, Eu, and Lu should exhibit chemistries similar to that of La and Pr.

Acknowledgment. The authors thank J. D. Corbett and M. H. Whangbo for helpful discussions. M.K. thanks G. Henkel for continuous support, the Deutsche Forschungsgemeinschaft for a postdoctoral fellowship (1995−1997), and the Alexander von Humboldt foundation (Germany, Bonn) for a Feodor-Lynen-"Nachkontakt" fellowship. This work was supported in part by the NSF CAREER award to J.D.M. (DMR-9501370).

Supporting Information Available: One X-ray crystallographic file, in CIF format. This material is available free of charge via the Internet at http://pubs.acs.org.

IC000986D